PAPER • OPEN ACCESS

Electronic work function modulation of phosphorene by thermal oxidation

To cite this article: Juan Gómez-Pérez *et al* 2022 *2D Mater.* **9** 015003

View the article online for updates and enhancements.

2D Materials

Electronic work function modulation of phosphorene by thermal oxidation

Juan Gómez-Pérez[1,*] , Cora Pravda Bartus[1], Ákos Szamosvölgyi[1], András Sapi[1] , Zoltán Kónya[1,2] and Ákos Kukovecz[1]

[1] Department of Applied and Environmental Chemistry, Interdisciplinary Excellence Centre, University of Szeged, H-6720, Rerrich Béla tér 1, Szeged, Hungary
[2] MTA-SZTE Reaction Kinetics and Surface Chemistry Research Group, H-6720, Rerrich Béla tér 1, Szeged, Hungary
[*] Author to whom any correspondence should be addressed.

E-mail: juan.gomez@chem.u-szeged.hu

Abstract

In this study, we evaluate the variation of the work function of phosphorene during thermal oxidation at different temperatures. The ultraviolet photoelectron spectroscopy results show an N-shaped behaviour that is explained by the oxidation process and the dangling-to-interstitial conversion at elevated temperatures. The exfoliation degree and x-ray photoelectron spectroscopy confirm the formation of native oxides in the top-most layer that passivates the material. *Ex-situ* XPS reveals the full oxidation of monolayers at temperatures higher than 140 °C, but few-layer phosphorene withstands the thermal oxidation even up to 200 °C with slight modifications of the A^2_g/A^1_g and A^2_g/B_{2g} vibrational mode ratios and a weak fluorescence in the Raman spectra of the heat-treated samples.

1. Introduction

Electronic and vibrational spectroscopies are important tools for the identification and quantification of oxidation. In recent literature, x-ray photoelectron spectroscopy (XPS) has been used for the identification of different types of phosphorene oxides predicted by computational studies [1, 2]: dangling and interstitial oxides (figure 1). Likewise, vibrational spectroscopy has been used to develop indicators for the detection of degradation or the degree of exfoliation by analysing the A^1_g, B_{2g}, and A^2_g vibrational mode ratios [3, 4] or blueshift, respectively.

Ultraviolet photoelectron spectroscopy (UPS) is used for the characterization of the electronic structure of a material. The work function and the information about occupied states close to the Fermi level can be used to evaluate the effects of oxidation or passivation by the interaction with other molecules [5]. Here, we investigate the use of UPS to characterize the oxidation of phosphorene by following the fluctuations of the energy required to release an electron from the Fermi level to the vacuum (i.e. the work function of phosphorene oxides) at intermediate oxygen concentrations.

The work function is an electronic property typically considered for the characterization of layered heterostructures [6], field emission devices [7] and energy conversion and storage devices [8, 9]. Similarly, the difference in work function between one metal and one semiconductor is used to explain the basic characteristics of heterojunctions and the formation or absence of potential barriers and depletion regions that describe the formation of Schottky or ohmic contacts (figure 2). The potential barrier affects the contact resistance with consequences on the carrier mobility and the ON-state current of field-effect transistors [10] but it also may improve the photocurrent efficiency [11, 12] thus its relevance for applications. Interestingly, the work function of a material not only describes intrinsic electronic properties, but it has been correlated to bulk mechanical properties like Young's modulus [13, 14], yield strength [15], ductility, and fracture toughness [16] in transition metals. These results have led to an increasing interest in the evaluation of mechanical
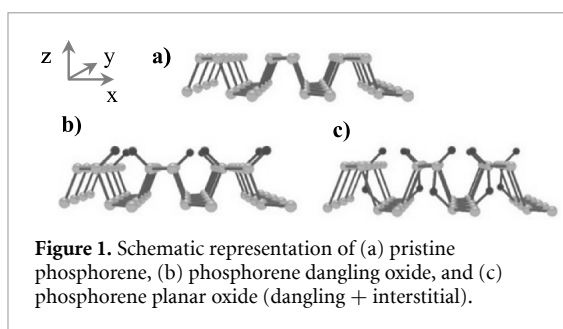
Figure 1. Schematic representation of (a) pristine phosphorene, (b) phosphorene dangling oxide, and (c) phosphorene planar oxide (dangling + interstitial).
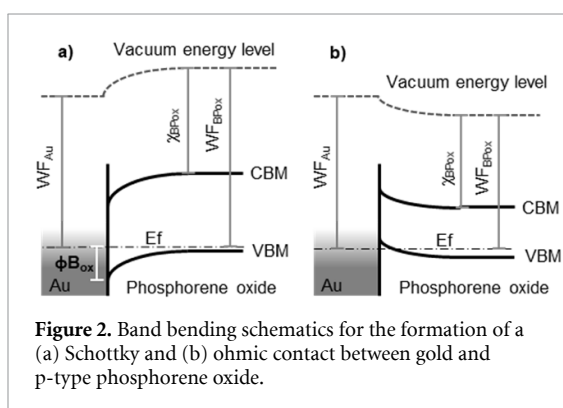

Figure 2. Band bending schematics for the formation of a (a) Schottky and (b) ohmic contact between gold and p-type phosphorene oxide.

Table 1. Comparison of the work function and energy barriers for oxidation in selected 2D materials.

Monolayer	Energy barrier[a] (eV)	Work function[b] (eV)
Graphene	2.2–2.7 [28]	4.56 [29]
MoS_2	0.93 [30]–1.6 [31]	5.15 [32]
$MoSe_2$	0.71 [30]	4.30 [33]–4.57 [34]
WS_2	0.86 [30]	4.73 [34]
h-BN	1.2–2.6 [35]	5.5–5.8 [17]
Phosphorene	0.1–0.5 [36, 37]	5.16 [22]

[a] Energy barrier for the formation of the transition state during oxidation.
[b] Pristine material.

properties of nanomaterials in correlation to their electronic properties [17–19].

On the other hand, 2D materials exhibit interesting features as their electronic properties can vary significantly by changing the number of layers of exfoliated materials. Few-layer phosphorene, a p-type 2D semiconductor obtained from the black phosphorus allotrope in 2014 [20], has been predicted to have one of the largest variations of the band gap [21] starting from the infrared with a value of 0.3 eV for the bulk material (i.e. samples thicker than 10 nm) and up the visible range of the spectra with 2.1 eV for the monolayer [22]. Additionally, it has large variations for the position of the conduction band minimum and the valence band maximum (VBM) depending on the number of layers. The work function varies between 4.5 and 5.5 eV depending on the number of layers [7], and more importantly, it is at the same energy level as the metals used for interdigitated electrodes. Hence, the number of layers and the variation of the electronic structure defines the charge transfer between phosphorene and metals in electronic devices and applications.

Despite the interesting properties described before, phosphorene is more easily oxidized than other 2D materials (table 1) [23] and the electronic properties of a material are not constant as they change easily by chemical processes encountered in real applications like catalysis, sensors, high-frequency transistors, etc where not only high temperature but other gases may be present at the surface of the material. The formation of phosphorene oxide has the lowest dissociation energy in comparison with graphene or MoS_2 which explains the rapid and

exothermic degradation of exfoliated materials in ambient conditions. Different approaches have been explored to attend this issue: chemical functionalization [24], intercalation [25], and defects engineering [6]. Nevertheless, the relationship between the different types of oxides and the work function has not been reported yet.

In this study, we find that native oxides effectively passivate the surface of a few-layer phosphorene and the oxidation process induces a modulation of the work function that follows an N-shaped curve. This result describes the experimental observations from previous reports [26, 27] showing the lattice expansion for the allocation of interstitial oxygen and the ohmic-to-Schottky-to-ohmic behaviour with interdigitated electrodes.

2. Methods

For the exfoliation of black phosphorus, a bulk crystal was purchased from HQ Graphene (Groningen, The Netherlands) and kept in an argon atmosphere. Ultrasonication of 4 mg in 10 ml of acetone was performed for 24 h at a controlled temperature of 25 °C in an Argon flushed atmosphere. After sonication, the supernatant was collected and centrifuged at 2000 and 4000 rpm for 30 min to obtain the supernatants labelled as BP2S and BP4S, respectively. From the UV–vis spectra (UV-3600 Plus, Shimadzu), optical band gaps were calculated and compared against previous experimental and theoretical results to evaluate the exfoliation degree. The thickness distribution was measured by Atomic Force Microscopy (AFM, PSIA XE-100, Park Systems Corp., South Korea) operated in tapping mode (cantilever: NSG30, radius of curvature: 10 nm, NT-MDT). A more complete description and characterization for the obtained suspensions has been included somewhere else [38]. For the dynamic light scattering characterization, a refractive index of 3.4 for exfoliated phosphorene was used.

The survey spectra from the XPS were collected using an Al Kα x-ray source (150 W, 14 kV) with

a pass energy of 40 eV and high-resolution spectra were collected with a pass energy of 20 eV. Additionally, investigation of the electronic properties of the samples was done with UPS (Excitation source He I. hv = 21.22 eV) with a bias of 8 V applied to the samples. The Fermi level was determined from the low kinetic energy region of the spectra. The work function (φ) was calculated as the difference between the incident photon and the spectrum width (W) by using the equation $\varphi = \text{hv} - W$, where W is the difference between the Fermi level and the secondary electron cut off.

The Raman spectra were collected with a Bruker, Senterra II instrument equipped with a 532 nm excitation wavelength and a 50x optical objective. The nominal laser power was 2.5 mW. The sample was drop cast on a silicon wafer with a sharp vibrational band at 520 cm^{-1} and a broad feature between 800 and 900 cm^{-1}.

3. Results

The BP4S and BP2S suspensions were characterized by dynamic light scattering and UV–Vis to determine the average hydrodynamic size and optical band gap. The results in table 2 indicate that the sample BP4S is composed mainly of monolayers, while the sample BP2S has monolayers, bilayers, and up to five-layer thick sheets. These results are congruent with the AFM results in figure 3.

Previously, the oxidation of phosphorene has been related to the detection of endothermic processes, variations in the Raman spectrum [27], and Schottky-to-ohmic transitions in the current–voltage characteristics [26]. Particularly, *In-situ* Raman measurements indicate a large deformation in the *c* direction of the lattice by a larger than expected red-shift of the A^1_g mode at high temperatures. This can be used as a proxy indicator of the presence of interstitial oxygen using vibrational spectroscopy, but clear electronic evidence was missing or sometimes contradictory. Later on, computational studies show that interstitial oxygen unlike dangling is characterized by a smaller work function and the difference between both species can be as large as 1 eV, thus it was easily traced using current–voltage characteristics [26]. Nevertheless, the previous measurements of current–voltage characteristics at different temperatures are an indirect method to analyse the impact of the electronic structure in the charge transfer process, but here we have collected new spectroscopic evidence by the combination of UPS and XPS to directly trace the modifications of the work function caused by the oxidation process in phosphorene.

For the XPS and UPS investigation, the samples were heated *ex-situ* in vacuum for 5 min at the desired treatment temperature. Next, the sample was let to reach room temperature and then it was characterized by XPS and UPS. After, the samples were heated

Table 2. Characterization of exfoliated phosphorene obtained by liquid-phase exfoliation in acetone.

Sample	Band gap (eV)	Average length (nm)[a]	Average thickness (nm)
BP2S	1.78	121 ± 20	4.0 ± 2.32
BP4S	2.05	99 ± 30	1.4 ± 0.49

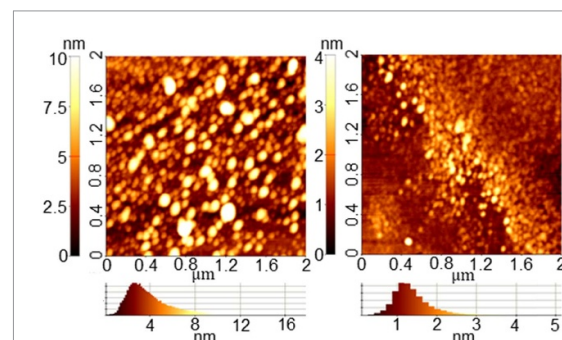[a] Hydrodynamic size.

Figure 3. AFM characterization. Right: BP2S. Left: BP4S. Thickness histograms below each corresponding image.
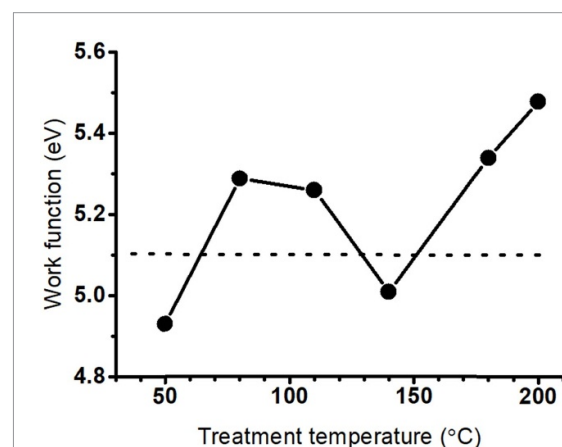

Figure 4. Work function of phosphorene oxides at room temperature after heat treatment at different temperatures. Dashed line: work function of gold at room temperature for comparison.

again to the next treatment temperature and the process was repeated. The temperatures evaluated were 50 °C, 80 °C, 110 °C, 140 °C, 180 °C, and 200 °C. The results are shown in figure 4.

The variation of the work function follows an N-shaped curve characterized by an initial increase of the work function then followed by a change in the tendency and decay of approx. 0.5 eV. Finally, it increases to values of work function larger than 5.0 eV. For comparison, the work function of gold is 5.1 eV at room temperature [39]. Gold is a common material for electrodes in optoelectronic devices, sensors, etc so here we demonstrate that the charge transfer and contact resistance between at the Au/BP interface may suffer fluctuations directly related to

the type of oxide in a fashion that is not predictable as for the majority of materials, oxidation results in a monotonic increase of the work function [40]. In perspective, the magnitude of this fluctuation is equivalent to the reported values in graphene oxide and reduced graphene oxide, where the increased oxygen concentration resulted in an increased work function of approx. 0.5 eV [41], but unlike other materials, in phosphorene it is not monotonic.

For a p-type semiconductor, the contact with a gold surface will form an ohmic contact when the work function of the semiconductor is smaller than the work function of gold, otherwise, the contact will be Schottky as depicted in figure 2. In the case of phosphorene, it means that depending on the degree of exfoliation increased contact resistance (supporting information, figure S3 available online at stacks.iop.org/2DM/9/015003/mmedia) is a signal of dangling-to-interstitial transition. Additionally, because the results in figure 4 are taken from spectra collected at room temperature it also indicates that the interstitial oxides are stable at room temperature, unlike a previous report where *in situ* current–voltage characteristics showed an increased contact resistance and the Schottky-to-ohmic transition characteristic of the formation of planar oxides [26].

Figures 4 and 5 show how the oxidation of phosphorene induces fluctuations of the work function that affect the performance of transducers and other applications based on phosphorene. The computational results for surface phosphorene oxides (dangling and interstitial oxides) show that the increasing concentration of oxygen in dangling position results in a higher work function while the conversion of dangling to interstitial oxides is characterized by a decay of the work function [26]. Fluctuations of the work function of phosphorene have been reported empirically at the early stages of oxidation [42]. In this work, spectroscopic evidence is used to explain the results in figure 4.

The P 2p region of the x-ray photoelectron spectra collected after the UPS measurements provides information about the oxidation process. In general, the samples were partially oxidized (figure 5). The deconvolution and the P(0) 3/2, PO*x* 3/2 ratio indicate an oxidation degree of $34.5 \pm 4.2\%$. The standard deviation of 4.2% indicates that the amount of new oxygen incorporated (chemisorption) into the lattice is low, thus, we assume that the variations of the work function are due to the differences in the electronic structure of the different types of oxides (i.e. dangling oxygen and interstitial oxygen). After the heat treatment, shifting of the peaks was detected as shown in figure 6.

At temperatures higher than 100 °C the chemical shift (i.e. Δ_{Energy} of the different chemical forms) for P(0) 1/2, PO*x* 1/2, and P(0) 3/2, PO*x* 3/2 increases monotonically but at temperatures higher than 180 °C it is stabilized. If we assume surface

oxides as the predominant form at low temperature and planar oxides (dangling + interstitial) at 200 °C, then we can estimate that the energy involved in the chemical reaction for the formation of planar oxides is equal to $\Delta E \cong 0.45$ eV (thermodynamic reaction energy). Computationally, it was calculated that the dangling-to-interstitial process is exothermic but has a required activation energy of 0.69 eV [36]. These experimental results support the computational findings with the differences explained by electrostatic repulsion.

By comparison of the x-ray photoelectron spectra from the samples BP2S and BP4S, the difference in stability is noticeable. The atomically-thin exfoliated phosphorene (BP4S) is fully oxidized at the temperature of 180 °C, however, under similar conditions, the sample BP2S withstood the thermal oxidation and P(0) features were practically unaltered at 200 °C. These results support the argument that native oxides can passivate the material and inner layers are effectively protected at least during the early stages of oxidation.

The precise identification of the different types of oxides requires high-resolution spectra to distinguish the fine differences produced by interstitial or dangling oxides. For example, with synchrotron-based XPS are noticeable the features relative to phosphorus in the O–P=O or P–O–P configuration at 132.8 and 131.5 eV, respectively [1], but these features are challenging to observe with lower resolutions. However, in measurement from another batch, we were able to identify an increased intensity of the interstitial (P–O–P) and planar (P–O–P=O) oxides at high temperatures close to the complete thermal degradation (figure 7), which is in agreement with previous Raman results [27] and the assumptions made in this report.

The most stable oxide (phosphorus pentoxide, P_2O_5) is expected at temperatures higher than 200 °C or in fully oxidized samples. The work function of P_2O_5 can be predicted by applying chemical and theoretical approaches using electronegativity concepts [43]. These predictions have been tested with experimental data and proven accurate with R^2 of 0.91 for a series of binary oxides [40]. A work function of 9.6 eV can be estimated for P_2O_5 utilizing a phosphorus electronegativity of 2.19 Pauling units, or even higher (10.0 eV) considering a cation electronegativity of 2.10 Pauling units [44]. Experimentally, it has been measured that the electronic work function of oxidized few-layers black phosphorus is approx. 8.2 eV [1]. The difference may be caused by the presence of metastable oxides that may reduce the overall result.

After the photoelectron spectral measurements, the Raman spectra for the samples at room temperature confirm the complete degradation of the sample BP4S and possibly the formation of P_2O_5, the most stable phosphorus oxide. The complete degradation of monolayers occurred after short
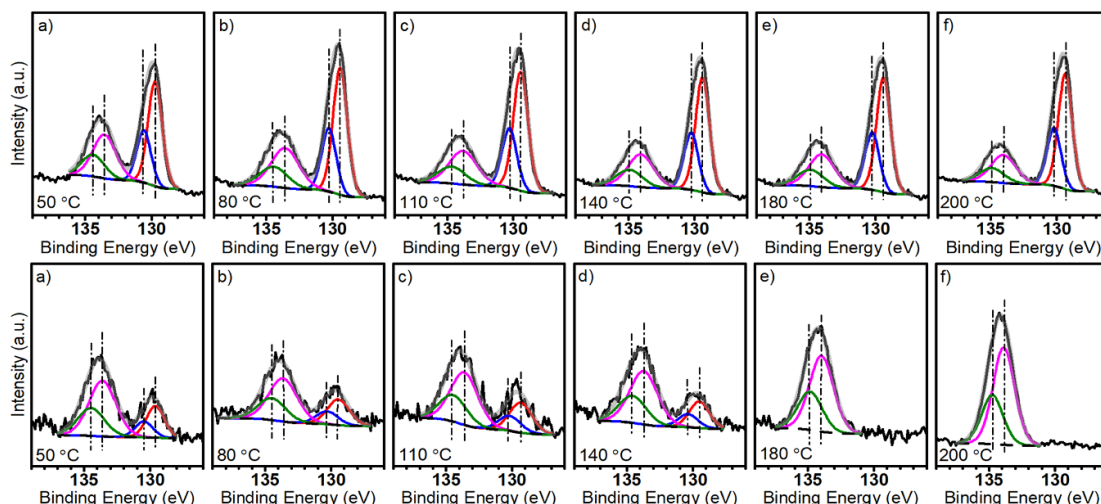
Figure 5. XPS measurements at room temperature for samples BP2S (top) and BP4S (bottom) after thermal treatment for 5 min at the indicated temperature.
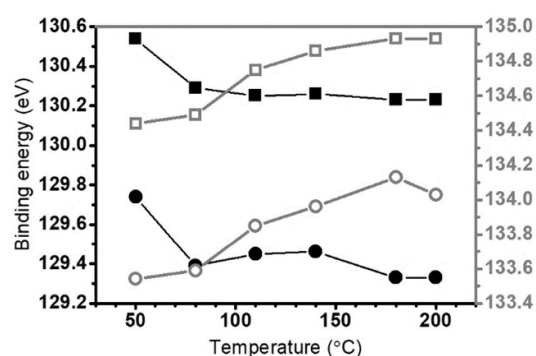

Figure 6. Binding energies for ■ P(0) 1/2, ● P(0) 3/2, □ PO*x* 1/2 and ○ PO*x* 3/2 after selected treatment temperatures. Sample BP2S.

Figure 8. Raman characterization for the sample BP2S before (top) and after the XPS, UPS measurements. Inset: detail for the vibrational region of BP.
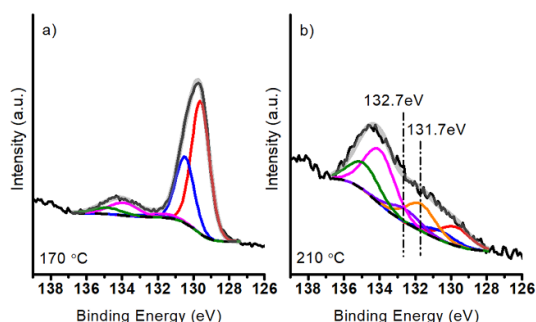

Figure 7. XPS measurements at room temperature after heat treatments at (a) 170 °C and (b) 210 °C.

exposures at temperatures higher than 140 °C and it has practical implications because the most common solvents for liquid-phase exfoliation (e.g. N-methyl-2-pyrrolidone, Dimethylformamide, Dimethyl sulfoxide) have boiling points higher than 150 °C. On the other hand, the sample BP2S retains the 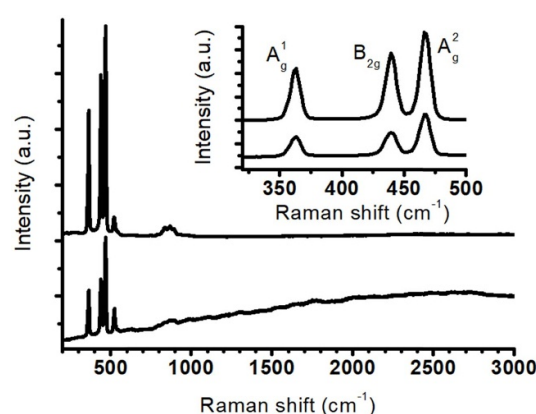vibrations of black phosphorus and develops other features (i.e. fluorescence) attributable to phosphorus oxides acting as a passivation layer (figure 8).

Raman intensity describes the polarizability and symmetry of amorphous and crystalline materials; thus, it is used to probe the bonding covalence and structure [45]. In figure 8, the A^2_g/A^1_g and A^2_g/B_{2g} vibrational mode ratios for the samples before and after the photoelectron experiments have slight differences. Before the heat treatments, the A^2_g/A^1_g and A^2_g/B_{2g} ratios were 0.59 and 0.76, respectively. After the heat treatment applied during the photoelectron experiments, the A^2_g/A^1_g and A^2_g/B_{2g} ratios were 0.48 and 0.56, respectively. These variations can be attributed to the lattice deformation (symmetry) and the change in polarizability caused by the chemisorption of oxygen in different positions. The vibrational energy was kept relatively constant with Raman shifts for the A^1_g, B_{2g}, and A^2_g at 362.5, 439.5, and 467.1 cm^{-1}, respectively. The latter may be explained

because the majority of the Raman signal probably comes from the pristine layers underneath the top-most oxidized layer [36].

4. Conclusion

The work function of phosphorene oxides has N-shaped fluctuations attributable to the formation of different types of oxides. These variations can be as large as 1 eV and affect phosphorene-based electronic devices as it occurs at similar energy levels as the Fermi level of gold or other metals commonly used for electrodes in optical or chemical transducers. These fluctuations affect the contact resistance, the ON-state current, or the charge carrier mobility in field-effect transistors, and it is also predicted to affect the mechanical properties of the material.

XPS measurements show the ability of native oxides to passivate the surface of a few-layer phosphorene. In the case of monolayers, the rapid degradation to fully oxidized forms was observed. Under the same conditions, despite some signs of oxidation, few-layer phosphorene keeps the vibrational bands of the underneath flakes even after the heat treatment at 200 °C. Despite the possibility of electronic structure engineering by the formation of a native oxide layer, the formation of different types of oxides induces fluctuations of the work function and VBM that may impact positively or negatively the performance of the material for different applications.

The comparison between the electronic and vibrational spectroscopy (Raman) revealed some features that may be useful indicators for intermediate oxidation: weak fluorescence, and lower A^2_g/A^1_g and A^2_g/B_{2g} ratios but no evident blue or redshift after the heat treatment was noticed for the sample. The increment of the A^2_g/A^1_g and A^2_g/B_{2g} ratios is related to an increased chemical shift associated with the formation of interstitial oxides. The formation of interstitial oxides can be achieved by temperature or may be induced by electrostatic repulsion [2] at higher oxygen concentrations.

Data availability statement

All data that support the findings of this study are included within the article (and any supplementary files).

Acknowledgments

ORCID iDs

Juan Gómez-Pérez ⓘ https://orcid.org/0000-0002-2736-2015
András Sapi ⓘ https://orcid.org/0000-0001-6557-0731
Zoltán Kónya ⓘ https://orcid.org/0000-0002-9406-8596
Ákos Kukovecz ⓘ https://orcid.org/0000-0003-0716-9557

References

[1] Edmonds M T, Tadich A, Carvalho A, Ziletti A, O'Donnell K M, Koenig S P, Coker D F, Özyilmaz B, Neto A H C and Fuhrer M S 2015 *ACS Appl. Mater. Interfaces* **7** 14557–62
[2] Ziletti A, Carvalho A, Trevisanutto P E, Campbell D K, Coker D F and Castro Neto A H 2015 *Phys. Rev. B* **91** 085407
[3] Abellán G, Wild S, Lloret V, Scheuschner N, Gillen R, Mundloch U, Maultzsch J, Varela M, Hauke F and Hirsch A 2017 *J. Am. Chem. Soc.* **139** 10432–40
[4] Abellán G, Lloret V, Mundloch U, Marcia M, Neiss C, Görling A, Varela M, Hauke F and Hirsch A 2016 *Angew. Chem., Int. Ed.* **55** 14557–62
[5] Guo R *et al* 2019 *Appl. Surf. Sci.* **496** 143688
[6] Lin Z *et al* 2016 *2D Mater.* **3** 042001
[7] Madas S, Mishra S K, Kahaly S and Kahaly M U 2019 *Sci. Rep.* **9** 1–11
[8] Pang J, Bachmatiuk A, Yin Y, Trzebicka B, Zhao L, Fu L, Mendes R G, Gemming T, Liu Z and Rummeli M H 2018 *Adv. Energy Mater.* **8** 1–43
[9] Cheng J *et al* 2020 *Nano-Micro Lett.* **12** 1–34
[10] Song S M, Park J K, Sul O J and Cho B J 2012 *Nano Lett.* **12** 3887–92
[11] Xia F, Mueller T, Golizadeh-Mojarad R, Freitage M, Lin Y-M, Tsang J, Perebeinos V and Avouris P 2009 *Nano Lett.* **9** 1039–44
[12] Garg R, Dutta N and Choudhury N 2014 *Nanomaterials* **4** 267–300
[13] Lu H, Liu Z, Yan X, Li D, Parent L and Tian H 2016 *Sci. Rep.* **6** 1–11
[14] Rahemi R and Li D 2015 *Scr. Mater.* **99** 41–44
[15] Hua G and Li D 2012 *Phys. Status Solidi Basic Res.* **249** 1517–20
[16] Hua G and Li D 2016 *Phys. Chem. Chem. Phys.* **18** 4753–9
[17] Thomas S, Manju M S, Ajith K M, Lee S U and Asle Zaeem M 2020 *Physica* E **123** 114180
[18] McCreary A, Kazakova O, Jariwala D and Al Balushi Z Y 2021 *2D Mater.* **8** 013001
[19] Losi G, Restuccia P and Righi M C 2020 *2D Mater.* **7** 025033
[20] Liu H, Neal A T, Zhu Z, Luo Z, Xu X, Tománek D and Ye P D 2014 *ACS Nano* **8** 4033–41
[21] Kovalska E, Luxa J, Hartman T, Antonatos N, Shaban P, Oparin E, Zhukova M and Sofer Z 2020 *Nanoscale* **12** 2638–47
[22] Cai Y, Zhang G and Zhang Y-W 2014 *Sci. Rep.* **4** 6677
[23] Wang G, Pandey R and Karna S P 2017 *Wiley Interdiscip. Rev.-Comput. Mol. Sci.* **7** 1–6
[24] Liu Y, Chen M and Yang S 2021 *InfoMat* **3** 231–51
[25] Xu G, Liu Y, Hong J and Fang D 2020 *2D Mater.* **7** 1–8
[26] Gómez-Pérez J F, Correa J D, Pravda C B, Kónya Z and Kukovecz Á 2020 *J. Phys. Chem. C* **124** 24066–72
[27] Gómez-Pérez J, Barna B, Tóth I Y, Kónya Z and Kukovecz Á 2018 *ACS Omega* **3** 12482–8
[28] Ni S, Li Z and Yang J 2012 *Nanoscale* **4** 1184–9
[29] Yan R *et al* 2012 *Appl. Phys. Lett.* **101** 1–4

[30] Liu H, Han N and Zhao J 2015 *RSC Adv.* **5** 17572–81

[31] Kc S, Longo R C, Wallace R M and Cho K 2015 *J. Appl. Phys.* **117** 135301

[32] Choi S H, Shaolin Z and Yang W 2014 *J. Korean Phys. Soc.* **64** 1550–5

[33] Borodin B R, Dunaevskiy M S, Benimetskiy F A, Lebedev S P, Lebedev A A and Alekseev P A 2018 *J. Phys.: Conf. Ser.* **1124** 6–11

[34] Haastrup S *et al* 2018 *2D Mater.* **5** 042002

[35] Zhao Y, Wu X, Yang J and Zeng X C 2012 *Phys. Chem. Chem. Phys.* **14** 5545–50

[36] Ziletti A, Carvalho A, Campbell D K, Coker D F and Castro Neto A H 2015 *Phys. Rev. Lett.* **114** 26–29

[37] Wang G, Pandey R and Karna S P 2015 *Nanoscale* **7** 524–31

[38] Gómez-Pérez J, Kónya Z and Kukovecz Á 2018 *Nanotechnology* **29** 365303

[39] Kahn A 2016 *Mater. Horiz.* **3** 7–10

[40] Greiner M T, Chai L, Helander M G, Tang W-M and Lu Z-H 2012 *Adv. Funct. Mater.* **22** 4557–68

[41] Kumar P V, Bernardi M and Grossman J C 2013 *ACS Nano* **7** 1638–45

[42] Kim M, Kim H, Park S, Kim J S, Choi H J, Im S, Lee H, Kim T and Yi Y 2019 *Angew. Chem., Int. Ed.* **58** 3754–8

[43] Nethercot A H 1974 *Phys. Rev. Lett.* **33** 1088–91

[44] Matar S F, Campet G and Subramanian M A 2011 *Prog. Solid State Chem.* **39** 70–95

[45] Colomban P and Slodczyk A 2009 *Opt. Mater.* **31** 1759–63